A Characterization of Laser Cleaning Painting Layer From Steel Surface Based on Thermodynamic Model

yao lu
Harbin Institute of Technology
ye ding (848590071@qq.com)
Harbin Institute of Technology
maolu wang
Harbin Institute of Technology
lijun yang
Harbin Institute of Technology
yang wang
Harbin Institute of Technology

Research Article

Keywords: Laser cleaning, Microstructures, Mechanical properties, Cleaning threshold, Cleaning mechanism

Posted Date: February 23rd, 2021

DOI: https://doi.org/10.21203/rs.3.rs-224748/v1

Version of Record: A version of this preprint was published at The International Journal of Advanced Manufacturing Technology on July 6th, 2021. See the published version at https://doi.org/10.1007/s00170-021-07566-6.

A characterization of laser cleaning painting layer from steel surface based on thermodynamic model

Yao Lu[b], Ye Ding[a,b*], MaoLu Wang[a,b], LiJun Yang[a,b*], Yang Wang [a,b]

a. Key Laboratory of Micro-systems and Micro-structures Manufacturing, Ministry of Education, Harbin Institute of Technology, Harbin 150001, China

b. School of Mechatronics Engineering, Harbin Institute of Technology, Harbin 150001, China

ABSTRACT

In this study, the environmentally friendly nanosecond ultraviolet (UV) laser is innovatively employed laser cleaning to remove the painting layer from the AH36 steel substrate. The feasibility of UV laser cleaning the painting layer is innovatively proposed and it has been calculated by the model theoretically, followed by elaborating the prominent interaction mechanism of UV laser exactly. The initial cleaning threshold and completely cleaning threshold are 2 J/cm^2 and 5 J/cm^2, respectively. Afterwards, the UV laser cleaned surface quality is evaluated by the scanning electron microscopy (SEM), energy dispersive spectroscopy (EDS), optical microscopy (OM) and optical profiler (OP), respectively. The mechanical properties have enhanced dramatically after laser cleaning and characterized by the Vickers hardness tester and universal testing machine. By varying laser fluences (2, 5, 7 J/cm^2) during laser cleaning, microstructures registering various sizes of corrugated shaped, craters and ring-shaped could be acquired. In addition, the mechanical properties analysis including rapid melting, quenching and dislocation density effects illustrates that laser cleaning could effectively increase surface microhardness, tensile strength and bending strength. Thus, laser cleaning method has emerged as a favourable means to strip painting layer in lieu of traditional methods for marine industry as well as this study could promote the development of laser cleaning in the field of marine engineering.

Keywords: Laser cleaning; Microstructures; Mechanical properties; Cleaning threshold; Cleaning mechanism

* Corresponding author. E-mail: dy1992hit@hit.edu.cn (Y. Ding), yljtj@hit.edu.cn (L. Yang)

1. INTRODUCTION

In the past a few decades, surface cleaning has been attracting considerable attention in various fields including aerospace, ocean engineering, microelectronics and medicine [1-4]. With regard to the contaminants on the surface, they are mostly of oxides, paints, polymers, coatings, microorganisms and particles [5-10]. Marine ships defouling the painting layer is a significant concern, which is mainly due to the corrosion as exposed to seawater. In this regard, ships appear to experience the paint removing alongside repainting for the maintenance of shipyard. Of particular note, the above issue has been reported to cost billions of dollars annually. Therefore, it is vital to strip off the painting layer from the substrate in order to repainting and extending the service life of the ship. Seen from prior studies, the traditional surface cleaning methods including the mechanical and chemical cleaning are recognized to be the most popular approaches. However, they have been reported to trigger the risks of polluting atmosphere and producing secondary wastes. Standing on this view, the laser cleaning method, emerging as a promising technique, is recognized to be an alternative to those conventional methods as it is more eco-friendly and does not need to contact cleaned surface. Depending on a host of traits including but not limited to excellent plasticity and toughness, high mechanical strength alongside light density and fair stiffness, steel, e.g. type AH36, has been widely used in ocean engineering [11-13]. However, it should be emphasized here that the service life of devices made with steel is strongly affected by marine environment as the latter contains a large amount of erosive ions and microorganisms which may collaboratively trigger the spalling of painting layer coating the exterior of steel base. What in follows, the internal steel base is degraded as the subsequent exposure continues. Thus,

surface cleaning is extremely necessary as it allows to remove the old painting layer that has been damaged, together with the attaching erosive substances. There so far exist extensive studies to provide constructive hints for solving the above concern through laser cleaning technique. In 1974, J.A. Fox pioneered a study to conduct surface cleaning upon paint layer, which was essentially achieved by using a Q-switched neodymium laser [14]. It was reported that the paint layer can be removed effectively under the strong photo-induced stress wave generated by the associated laser. Besides, K. Liu and E. Garmire adopted different types of laser alongside varying pulse width to remove the lacquer [15]. Seen from that, the Nd: YAG laser along with Q modulation was reported to show the stronger removal effect in comparison to other examined lasers, i.e. CO_2 laser, excimer laser and continuous wave laser. More importantly, Chen et al. pointed out that the laser cleaning technique may overcome the main flaw existing in conventional cleaning methods, viz. secondary pollution, which was confirmed through optical microscope observation [13].

As is well reported, many factors including but not limited to the pulse frequency, the scanning line interval, the scanning speed and the laser fluence are able to affect the efficiency of laser cleaning [16-30]. According to Zhao et al., the energy incorporated in each single pulse increased as the pulse frequency decreased, which would potentially trigger the plasma shielding effect near the painting layer surface once the pulse energy reached to a certain value. Of particular note, this resulting plasma shielding effect has a potential to cause the recession phenomenon through absorbing the energy involved in lasers and accordingly, hinders the further cleaning effectiveness to the painting layer [17-19]. Besides, the larger scanning line interval was reported to decrease the corresponding cleaning efficiency. This may be attributed to that the increase in the

scanning interval could dilute the unit received energy or fluence at the scanned region on the one hand and sometimes even leads to the appearance of residual area on the second hand [20-23]. In addition, the scanning speed influence the cleaning efficiency essentially through changing the corresponding overlapping rate. In this regard, the larger scanning speed, the better cleaning performance, and vice versa. [24,25]. Apart from the above, laser fluence has been widely recognized as a predominant factor when investigating the laser cleaning effectiveness [2, 4, 11, 26-30]. In an early study conducted by Tian et al., two different laser fluences, namely 1.08 J/cm^2 and 4.14 J/cm^2, were respectively set and the higher cleaning efficiency was noted in the case of larger laser fluence [4]. This has also been confirmed by a recent report [11], wherein the increase in laser fluence within a certain range, from 1.19 J/cm^2 to 4.43 J/cm^2, was once again noted to help improve the corresponding cleaning efficiency. The underlying reasons behind this may be that the increasing fluence empowers the thermodynamic behavior of molecules and accordingly make the attached contaminants easier be removed after a series of process including melting, vaporizing, solidifying. As well, the larger fluence allows to produce the plasma in a quicker and more efficient way, which also favors the further cleaning [2,11]. However, it should be emphasized here that any increase in laser fluence beyond a threshold might trigger a risk of damaging the substrate. For instance, such an upper bound in terms of laser fluence was reported to be about11.9 W/cm^2, which induces the excessive ablation of the substrate [31-33]. Together with experimental investigations, numerical simulations have also been extensively carried out to understand the underlying mechanism involved in laser cleaning. W.F. Zou et al. established a one-dimensional heat conduction model based on the thermal stress mechanism alongside the Fourier transfer equation.

Then, the process of laser cleaning was successfully simulated and the cleaning and damage thresholds were so numerically predicted [34]. On the basis of heat conduction and Hertz-Knudsen theory, V. Oliveira et al. developed a 2D finite element model to describe the TiC ablation effects led by pulsed laser irradiation with varying laser fluence, and the corresponding results agreed well with pertinent experimental values [35]. Aside from this, Vasantgadkar et al. also predicted the ablation depth and temperature distribution, on account of plasma shielding effect [36]. Yue et al. adopted the laser respectively shaped as rectangular and Gaussian to numerically investigate the associated effect upon the cleaning efficiency [37].

However, it should be emphasized here that the laser employed in most of above studies were infrared nanosecond laser, that usually triggers thermal induced defects, manifesting as the recasting layer and the heat-affected zone (HAZ). On the other hand, the ultraviolet (UV) laser may avoid these disadvantages effectively as it registers a greater photon energy and accordingly is easier to break the intermolecular bonds. To the authors' knowledge, there exists very limited study that adopted UV laser to clean the painting layer and more importantly, the influence led by associated parameters upon cleaning efficiency is still not clear. In this study, the authors mark the first in using UV laser to clean the painting layer and varying laser fluence levels ranging from 2 J/cm^2 to 7 J/cm^2 were examined. Further, the resulting samples were also evaluated through Optical Microscopy (OM), Field Emission Scanning Electron Microscopy (SEM), Optical Profiler (OP) and mechanical measurements.

2. EXPERIMENTAL

2.1 materials

A commercially sourced AH36 steel, as widely used in marine engineering, was employed as the substrate in this study, and its elementary compositions as determined by XRF technique is now presented in **Table 1**. A locally supplied paint comprising chlorinated rubber was used to coat the substrate twice. Note here that the inter layer (white color) registered a thickness of 70 μm while the outer layer (red color) was as thick as 100 μm. The dimensions of specimens, as being used to experience laser cleaning and further characterization including SEM-EDS, OP and OM, were set as 40 mm × 40 mm ×5 mm. In addition, another two batches of specimens, respectively sized as 40 mm × 5 mm ×5 mm and 30 mm × 10 mm ×2 mm, were prepared as well for tensile and bending tests, conforming to ASTM E8 and ASTM E290. The representative samples are illustrated in **Fig. 1**.

2.2 UV Laser cleaning surface treatment

For starter, the laser cleaning process is operated in an ambient atmosphere, i.e. (20℃), using a nanosecond fiber laser (Huaray, China) coupled with a two-dimensional galvanometer scanning system alongside the progressive scanning mode. The parameters in terms of employed laser were set as follows: maximum average power= 20 W, wavelength = 355 nm, laser pulse width = 15 ns, and laser repetition rate =100 kHz. Furthermore, three different laser fluences were examined, respectively corresponding to 2 J/cm^2, 5 J/cm^2, and 7 J/cm^2.

2.3 Surface characterization

The morphology of resulting specimens was characterized by a digital ultra-depth-of-field microscope (Keyence, VHE-1000, Japan) and a Field-Emission Scanning Electron Microscope

(FE SEM) coupled with an Energy Dispersive X-ray Spectroscope (EDS). The EDS was performed to analyze the chemical compositions of laser cleaned surface and the original painting layer surface. An optical profiler (OP, Zygo Corporation, USA) was adopted to evaluate the surface roughness and 3D morphology. In addition, the mechanical performance, i.e. tensile and bending strength, were measured through the Instron 5569 universal testing machine, which offered the uniaxial tension and 3-point approach bending tests. The microhardness was determined using the Vickers durometer.

3. RESULTS AND DISCUSSION

In order to realize the UV laser cleaning the painting layer feasibility, the underlying analysis and discussion are crucial and essential factors to obtain the outstanding laser cleaned effects theoretically. As for the mechanisms of UV laser cleaning, it is widely recognized that the photothermal, photochemical interactions and combination of them are underscoring effects, which has been expressed in various models detailly [38-45]. It is worth pointing out that during the period of laser cleaning, the photochemical interactions, viz. the energy of UV laser emitted photons are greater than the molecular bond energies within the material, which in turn further break the molecular bonds and manifest as the cold machining. One notes from the **Table 2**. that the detailed information as per the molecular bond energies of the painting layer. The photon energy is expressed as $E=h\gamma=hc/\lambda$, where E is photon energy, h is Planck constant, γ and λ are frequency and laser wavelength respectively. According to the theoretical calculation, the energy of 355 nm UV laser is 6.2 eV, which is much greater than molecular bond energies of the painting

layer, thereafter inducing molecular bonds broken chemically. It is well agreed with the prior mentioned theory and can be verified by theoretical calculation. From the table, it is clear that the energy of photon emitted by the UV laser (6.3 eV) is considerably greater than that most of molecular single bond, such as C-H bond registering 4.30 eV. Therefore, the adopted UV laser cleaning could remove the painting layer in theory by calculation of photon energy.

3.1 Surface morphology

One notes from **Fig. 2** that the representative images of laser cleaned surface are exhibited at varying laser fluence upon the painting layer adhered on the surface of AH36 steel substrate. It is noteworthy that there exists a strong smell of burning and a huge sound of vibration during the period of laser cleaning, which is mainly due to the interactions of the UV laser and the painting layer. Aside from this, it can also be inferred that both photothermal and photochemical reactions trigger on the surface of the painting layer. It is coincidence with the aforementioned theoretical analysis, namely, there exists both the photochemical and photothermal interactions showing up in the laser cleaning process, along with breaking molecular bonds chemically. Typically, **Fig. 2** (a, e, i) display the original painting layer surface before laser cleaning, while **Fig. 2** (b, f, j), (c, g, k) and (d, h, l) indicate laser cleaned surface at varying laser fluence of 2 J/cm^2, 5 J/cm^2, and 7 J/cm^2 respectively. Interestingly, seen from the **Fig. 2** (b), it can be shown that the superficial color changes on the surface, viz., different from red painting layers, which is due to the fact that there exist two kinds of painting layer (red and white) adhering on the substrate surface. After the laser cleaning at laser fluence of 2 J/cm^2, the red painting layer has almost been peeled off from the surface, whereas the white one left on the surface, as evident from **Fig. 2 (a)**. This may attribute

to the laser fluence cannot reach the threshold of the painting layer and the energy is not strong enough to remove the painting layer directly. Notably, the laser fluence at 2 J/cm^2 is called initial cleaning threshold. Aside from that, it worth mentioned here that there are some uncleaned areas at the edge of specimen after laser cleaning, which is mainly due to the laser satisfied Gaussian distribution in space, namely, the energy in the middle is evidently higher than the edges. As expected, the laser fluence distributed at the edges is not strong enough to strip the painting layer, which is coincide with the prior mentioned phenomena. One notes from **Fig. 2 (c)** that it can be presented a superficial color variation from the zebra like color to bar shaped grey-black color in the macro at a laser fluence of 5 J/cm^2. Specifically, UV laser cleaning induces a prominently complete removal and manifests as a metallic luster on the surface of the substrate. This may infer that improving the laser fluence could help enhance the laser cleaning effects and complete cleaning threshold of laser cleaning painting layer is 5 J/cm^2. The resulting surface indicates that the cleaning effects have positive correlation with laser fluence. Moreover, if the laser fluence increases to initial cleaning threshold, the painting layers begin to remove and there exists some traces on the surface. In contrast, if the laser fluence enhances to complete cleaning threshold, the corresponding painting layers are peeled off thoroughly. As noted earlier, the enhancement of laser fluence could promote the behavior of molecules thermodynamic and a host of process, the resultant surface is agreed well with previous study [11]. Compared with the laser cleaned surface at fluence of 5 J/cm^2, it can be found craters and tracks clearly in black color after the laser cleaning at a laser fluence of 7 J/cm^2, which is mainly due to existing the excessive ablation upon laser cleaned surface. This may be attributed to the photothermal effects play a prominent role in the

laser cleaning at a laser fluence of 7 J/cm^2 and the resultant surfaces may experience the evaporation, melting, re-solidification and ablation in an iterative dynamic process, which in turn further lead to the excessive ablation.

Fig. 3 exhibits a low magnification secondary electron SEM image of the micro-morphology of laser cleaned painting layer at varying laser fluence, including 2 J/cm^2, 5 J/cm^2 and 7 J/cm^2 respectively. For the captured surfaces observed in **Fig. 3** (a), the employed laser fluence was 2 J/cm^2 and it can be found there are some cracks and concaves exposed on the surface of laser cleaned surface, which is mainly due to the local temperature increase, viz. the enhanced lattice vibration induced cracking result in the temperature enhancement, which is coincide with the mechanism of the UV laser cleaning, namely, the photochemical interaction reactions between the laser and the painting layer. As noted from **Fig. 3** (d), instead of concaves and cracks, relatively smooth and evenly surface, viz. some corrugated shape morphology can be presented from the images, which indicates laser fluence reaching the cleaning threshold of the painting layer and without destroying the underlying substrate. The corrugated shape morphology is well agreed with a metallic luster surface of the substrate noted in **Fig. 2** (c), which is suggested that it is a thoroughly completely removal. As well, it is worth mentioning here that there are some ring-shaped microstructures showing up in **Fig. 3** (g). It is mainly due to the fact that the laser fluence exceeding the theoretical threshold considerably, which triggers the phase change of the substrate, followed by producing the ring-shaped microstructures. This is supported by the previous results [46]. Notably, there are many craters in each laser cleaned surface, as noted in **Fig. 3**, which may explain through the following: the AH36 steel substrate contains hydrogen. As for the UV laser

cleaning the surface of painting layer, it experiences melting, evaporation, rapid solidification and re-solidification as well as the corresponding hydrogen precipitates from the surface, followed by the formation of hydrogen. This is also supported by prior research results [5, 47]. In what follows, the craters cannot be filled with the liquid metal immediately, therefore it generates various craters microstructure on the surface of AH36 steel substrate.

3.2 Surface element distribution

For evaluating the laser cleaning painting layer effects, the energy dispersive X-ray spectroscopy (EDS) is widely recognized as a general method to examine the chemical composition. One notes from **Fig. 4** that it exhibits the corresponding elements content in the marked black box straightforwardly and the percentages of weight at varying laser fluence are expressed in **Table 3**. Together with the EDS analysis of the UV laser cleaned surface, the authors find that Fe element weight percentage is 53.04 % and oxygen is 5.58 % in weight percentage in area A. As noted from **Figs. 4 (a) and (b)**, compared with area A, the area B in the Fe and O element both have dramatically enhancement, which indicates area B has a relatively cleaned surface and exposed more substrate surface than area A. As seen therein, the process of area A belongs to incompletely cleaning period, whereas area B indicates it is a completely cleaning process, which is well agreed with the earlier mentioned **Fig. 3** (a) and (d), respectively. As for area C, it can be seen that the weight of C and O element higher than that of the area A and B, which suggests the area experiences excessive ablation and the corresponding iron oxide registers the ring-shaped microstructure. This is also agreed well with the aforementioned **Fig. 3** (g) phenomena, including the ring-shaped microstructure and the excessive ablation effects.

To reveal the surface element distribution more clearly, the line EDS is performed to investigate changes of Fe, O, C content along with some trace amounts of Cr and Ti. **Fig. 5** (a), (b) and (c) exhibit the line EDS report of element changes in the resulting laser cleaned area at varying laser fluence of 2 J/cm^2, 5 J/cm^2 and 7 J/cm^2 respectively. From the curves, it can be observed that the Fe Kα1 appeared in (a) and (c) oscillates significantly more than (b), which is mainly due to the laser cleaned surface (b) is relatively flat, viz. painting layer has been peeled off from the substrate completely. Interestingly, it can be found there are some periodic curves appearing in the line EDS examined surface in **Fig. 5** (a). This indicates that the produced the ring-shaped microstructure, namely, iron oxide is approximately periodic, which is due to the UV laser satisfied the Gaussian distribution.

One notes from **Fig. 6** (a) that presents a secondary electron SEM image of UV laser cleaned surface morphology and manifests as disparate contrasts areas thoroughly. In **Fig. 6** (b-g), it can be observed certain specific elements including Fe, O, C, Ni, Cr, and Mo are distributed on the surface with various colors. From the mapping of the AH36 steel substrate surface, it is presented the distribution of Fe, O and C is the major elements on the surface, which is mainly due to Fe and C elements are the prominent elements of substrate and there may exist the laser ablation during the laser cleaning period. Clearly, from the mapping, it can be seen the distribution of the O and C is relatively homogeneous. As per the surface morphology of laser cleaned surface, it is suggested that the convex exposed on the laser cleaned surface is rich in the O and C elements, whereas they are almost absent in the center. This may be attributed to the UV laser satisfied Gaussian distribution and the energy density at the center of the spot is greater than that at the edge, which

results in the O element exposed in the center much more the edges. That is the reason why the microstructure could generate the ring-shaped microstructure and corrugated shape morphology respectively. Herein, the present findings are very encouraging and it can also infer that the nanosecond UV laser could successfully strip off the painting layer thoroughly.

3.3 Mechanical properties analysis

3.3.1 Hardness characterization

It is widely recognized that evaluate the mechanical properties exactly, the hardness characterization is an indispensable, essential evaluation index, which needs to be considered during the UV laser cleaning the painting layer. In this study, the Vickers microhardness test is performed to investigate the mechanical properties, the details including the load of 290 g and holding time duration of 15 s, which can be demonstrated in **Fig. 7**. As such, from the curves, it can be noticed that the UV laser cleaned surface increases to 150 HV while the uncleaned surface is 92 HV. As for the dramatically microhardness enhancement can be attributed to the fact that the UV laser cleaned surface shows up rapid melting and quenching, which is followed by generating the microstructure, including ring-shaped and corrugated shaped. The other reason is due to the fact that the UV laser cleaning could induce the resultant surface producing dislocation density, while the traditional cleaning techniques are not available. This is supported by the previous results [17, 48, 49]. Specifically, the standard deviation of laser cleaned surface and uncleaned surface microhardness is 2.875 and 0.525, respectively. Due to the painting layer uneven, the maximum Vickers microhardness UV laser cleaned surface is 178 HV and the minimum is 150 HV. Thus, it is suggested that UV laser cleaning painting layers could enhance the surface microhardness

considerably. Aside from the environmentally friendliness, this is another reason why authors take this prospective method to remove the painting layer.

3.3.2 Tensile and bending characterizations

For further investigating the tensile and bending properties of laser cleaned surface, there are batches of standard tensile and bending test specimen produced by UV laser cleaning method. The commensurately tensile stress and strain curves are illustrated in **Fig. 8**. From the curves, it can be exhibited five stages in these tensile curves, such as elastic deformation, yield deformation, plastic deformation, necking and fracture respectively [50-56]. The curves are just like the parabolic shape and there is a rapid increase in the elastic and yield deformation stages. Followed by gradually enhanced to the plastic deformation stage, there exist maximum values, viz., ultimate strength appearing before reaching necking period, along with the reduction to facture stage sharply. Notably, the tensile strength of laser cleaned surface is much stronger than that of before cleaning, which is mainly due to the laser treatment is conducive to enhance the elastic and plastic deformation properties of the substrate.

As for bending properties, it is widely recognized bending displacements and bending stress are essential factors, which can be exhibited in **Fig. 9**. As noted in the curves, it can be observed that both of the resulting laser cleaned surface and uncleaned surface experience complete elastic deformation and plastic deformation stage, whereas the fracture stage does not exist in the sample, in spite of the bending angles exceeding 90° and bending stress over 1000 MPa. In this regard, it indicates that both of the laser cleaned surface and uncleaned surface have excellent bending strength and plasticity. Yet, laser cleaned surface manifests as better plasticity in the plastic

deformation stage. Thus, the laser cleaned surface conduces to improve the bending strength and plasticity properties.

3.3.3 Roughness and profile characterizations

As seen in **Fig. 10**, it presents typical 3D morphologies along with corresponding line scanned profiles of original painting layer and resulting laser cleaned surface, which is examined by optical profiler and commensurately captured zone is 840 μm × 840 μm. As evident from **Fig. 10** (a), it can be seen that the original painting layer is relatively evenly and smooth, along with the surface roughness 1.968 μm. Of particular note, white lines indicate maximum height difference is approximately 10 μm at original surfaces. With regard to the laser fluence 2 J/cm^2, the maximum height difference is five times larger than that of the original painting layer surface and corresponding surface roughness is 12.751 μm. This may be contributed to the laser energy is less capable to remove the painting layer directly and there exists laser cleaning induced cracks and concaves in this layer, which is well agreed with the prior mentioned **Fig. 3** (a). Thus, the roughness of laser cleaned surface at laser fluence 2 J/cm^2 increases dramatically. Specifically, as for laser cleaned surface at laser fluence of 5 J/cm^2, the resultant surface is pretty smooth, viz. the surface roughness is 2.471 μm and relevant maximum height difference is approximately 6 μm, which indicates laser fluence at 5 J/cm^2 is the most suitable for UV laser cleaning painting layers. As such, it is suggested that laser cleaned surface at this fluence without destroying the underlying substrate and the thermal ablation is minimal from the aforementioned surface morphology in **Fig. 3** (d). Therefore, laser fluence at 5 J/cm^2 is regarded as the threshold of UV laser cleaning painting layer. To be noted here, the melted layer flowing and re-solidification forms a corrugated shape

morphology, which coincides well with **Fig. 3** (d). In comparison, the laser cleaned surface at laser fluence 7 J/cm^2 has a relatively rough surface (6.298 μm) and the maximum height difference is about 27 μm, which is suggested that the surface experiences the excessive ablation and it is consistent with the captured images in **Fig. 3** (g). Thus, it is imperative to avoid the ablative conditions occurred during UV laser cleaning painting layer as far as possible.

3.4 Theoretical model analysis

The experimental results illustrate initial cleaning threshold and complete cleaning threshold based on laser and painting layer interactions. In order to explain the phenomena more detailly, it is necessary to establish a thermodynamic model to describe the laser cleaning mechanism. Based on the study of Zhang et al. [57], the theoretical relationship between the temperature and energy are expressed as:

$$\mathrm{E} = \mathrm{n} \cdot \left(\int_{T_1}^{T_2} c_P \, dT + \Delta \mathrm{H}\right) \quad (1)$$

Herein, T_1, T_2, n, C_P, ΔH stand for initial temperature, final temperature, amount of substance, heat capacity and molar heats of phase transition.

$$c_P = A + BT + CT^{-2} \quad (2)$$

Where, A, B, C are constants correlated with substance properties.

Based on the thermodynamic model, it is employed for theoretical calculation and the corresponding assumptions are under following conditions:

(a) The painting layer and AH36 steel substrate are taken as heat insulators.

(b) The distribution of laser energy is homogeneous.

One notes from **Fig. 11** that the schematic diagram of laser absorption and reflection. Wherein,

E_L, E_R, δ_1, δ_2 indicate incident laser energy, reflection laser energy and thickness of painting layer and substrate correspondingly. As well, E_{Fe}, E_A, E_B are energy absorption of Fe substrate, incident laser and reflection through painting layer respectively. A_a and A_b stand for laser absorption coefficients of painting layer and Fe substrate respectively. The detailed equations are shown as follows:

$$E_A = A_a \cdot E_I \tag{3}$$

$$E_{Fe} = A_b \cdot (E_I - E_A) \tag{4}$$

$$E_B = A_a \cdot (E_I - E_A - E_{Fe}) \tag{5}$$

Herein, α_1 and α_2 are laser absorption coefficients of painting layer and Fe substrate respectively. In addition, it can be calculated $\alpha_1 = (1 + (1 - A_a) \cdot (1 - A_b)) \cdot A_a$, $\alpha_2 = (1 - A_a) \cdot A_b$. As per Eq. (1), it can be obtained Eq. (6), as follows:

$$\alpha_1 E_I = \frac{\rho_1 \cdot s \cdot \delta_1}{M_1} \left(\int_{T_1}^{T_2} c_{P,painting}\, dT + \Delta H\right) \tag{6}$$

Afterwards, the laser fluence can be deduced from Eq. (7) and the relationship is expressed as:

$$F_1 = \frac{\rho_1 \cdot \delta_1}{\alpha_1 M_1} \left(\int_{T_1}^{T_2} c_{P,painting}\, dT + \Delta H_{painting}\right) \tag{7}$$

Correspondingly, the laser fluence of Fe substrate can be illustrated as follows:

$$F_2 = \frac{\rho_2 \cdot \delta_2}{\alpha_2 M_2} \left(\int_{T_1}^{T_2} c_{P,Fe}\, dT + \Delta H_{Fe}\right) \tag{8}$$

Wherein, ρ_1, ρ_2, M_1, M_2 are densities of painting layer and Fe substrate as well as molar masses of painting layer and Fe substrate, respectively.

Inspired from Eqs. (7), (8) and substituted the corresponding physical constants shown in

Table 4, it can be calculated the theoretical laser fluence is 1.789 J/cm^2 if temperature approaches its melting points. As for the Fe substrate, it also can be derived from functions that laser fluence are 3.216 J/cm^2 and 4.65 J/cm^2 with regard to the melting point and boiling point, respectively. It is noteworthy that the calculated theoretically threshold (4.65 J/cm^2) is exceeded initial cleaning threshold, which is mainly due to the fact that less consideration of the plasma shielding effects and thermal expansion effects as well as various thickness of painting layer. These points will be taken into account in future studies to modify this model effectively.

Comprehensively, the laser cleaning is a facile, environmentally friendly and promising method to strip off the painting layer from the marine engineering surface. Hopefully, this study would provide an experimental and theoretically analysis reference in the UV laser cleaning the painting layer and pave the way for any further potential applications in industrial field.

CONCLUDING REMARKS

In this paper, a study based on the nanosecond UV laser cleaning method is innovatively proposed, which is successfully utilized to strip off the painting layer from the AH36 steel substrate. This study innovatively verifies the feasibility of the UV laser cleaning the painting layer on the surface of AH36 steel in theory and briefly elaborates the primarily interaction mechanism of UV laser, such as the photothermal and photochemical interactions. The thermal dynamic model is established to describe the relationship between temperature and laser fluence, which indicates the experimental results (4.65 J/cm^2) are close to theoretical cleaning threshold (5 J/cm^2) and the differences between them are discussed exactly. Moreover, SEM, EDS, Optical profiler and

mechanical tests are detailly performed to study the morphologies, chemical compositions and mechanical properties of original painting layer surface and resulting laser cleaned surface at varying laser fluence respectively. From the SEM test, there are some typical corrugated shaped, craters and ring-shaped microstructures exhibited on the surface of laser cleaned surface at various laser fluence. With regard to the mechanical properties, it is worth mentioning here that the UV laser cleaned painting layer surface could enhance the surface microhardness, tensile strength and bending strength dramatically. This can be attributed to the UV laser cleaned surface experiencing rapid melting and quenching, followed by generating the ring-shaped and corrugated shaped microstructure as well as the produced dislocation density. Therefore, this promising UV laser cleaning method is not only environmentally friendly, but also enhances the mechanical properties of laser cleaned surface significantly. Hopefully, there is a great potential to utilize this promising method to large-scale cleaning the painting layer of the marine engineering surface and make some contributions to the marine and industrial fields in the future.

Acknowledgements

This research is supported by the National Key Research & Development Program (No. 2017YFB1105000) and Guangdong Province Key Area R&D Program (No. 2018B090905003). Yao Lu acknowledges the support and encouragement of Prof. Robert Fedosejevs at the University of Alberta.

Author's contributions

Yao Lu drafted this paper. Ye Ding and Maolu Wang supervise this manuscript. Lijun Yang and Yang Wang edit this paper. All authors approve this paper.

Declarations

Ethical approval Not applicable

Consent to participate Not applicable

Consent to publication All presentations of case reports have consent for publication

Declaration of Competing Interest

The authors declare that they have no known competing financial interests or personal relationships that could have appeared to influence the work reported in this paper.

REFERENCES

[1] F.D. Zhang, H. Liu, C. Suebka, Y.X. Liu, Z. Liu, W. Guo, Y.M. Cheng, S.L. Zhang, L. Li, Corrosion behaviour of laser-cleaned AA7024 aluminium alloy, Appl. Surf. Sci. 435 (2018) 452–461.

[2] T. Ze, Z.L. Lei, X. Chen, Y.B. Chen. Evaluation of laser cleaning for defouling of marine biofilm contamination on aluminum alloys. Applied Surface Science 499 (2020): 144060.

[3] L.Y. Yue, Z.B. Wang, L. Li, Material morphological characteristics in laser ablation of alpha case from titanium alloy, Appl. Surf. Sci. 258 (2012) 8065–8071.

[4] T. Ze, Z.L. Lei, X. Chen, Y.B. Chen. Nanosecond pulsed fiber laser cleaning of natural marine micro-biofoulings from the surface of aluminum alloy. Journal of Cleaner Production 244 (2020): 118724.

[5] T.Y. Shi, C.M. Wang, G.Y. Mi, F. Yan. A study of microstructure and mechanical properties of aluminum alloy using laser cleaning. Journal of Manufacturing Processes 42 (2019): 60-66.

[6] Mhaede M. Influence of surface treatments on surface layer properties, fatigue and corrosion fatigue performance of AA7075 T73. Mater Des 2012; 41:61–6.

[7] Qiang W, Guan Y, Cong B, Qi B. Laser cleaning of commercial Al alloy surface for tungsten inert gas welding. J Laser Appl 2016;28(2).

[8] Z.Y. Zhang, J.Y. Zhang, Y.B. Wang, S.S. Zhao, X.C. Lin, X.Y. Li, Removal of paint layer by layer using a 20 kHz 140 ns quasi-continuous wave laser, Optik 174 (2018) 46–55.

[9] M. Kumar, P. Bhargava, A.K. Biswas, S. Sahu, V. Mandloi, M.O. lttoop, B.Q. Khattak, M.K. Tiwari, L.M. Kukreja, Epoxy-paint stripping using TEA CO2 laser: Determination of threshold fluence and the process parameters, Opt. Laser Technol. 46 (2013) 29–36.

[10] Y. Lu, L.J. Yang, M.L. Wang, Y. Wang. Improved thermal stress model and its application in ultraviolet nanosecond laser cleaning of paint. Applied Optics 59.25 (2020): 7652-7659.

[11] Y. Lu, Y. Ding, G.W. Wang, L.J. Yang. Ultraviolet laser cleaning and surface characterization of AH36 steel for rust removal. Journal of Laser Applications 32.3 (2020): 032023.

[12] G. X. Chen, T. J. Kwee, K. P. Tan, Y. S. Choo, and M. H. Hong, High-power fiber laser cleaning for green shipbuilding, J. Laser Micro/Nanoeng. 7, (2012), 249–253.

[13] G. X. Chen, T. J. Kwee, K. P. Tan, Y. S. Choo, M. H. Hong, Laser cleaning of steel for paint removal, Appl. Phys. A (2010) 101, 249–253.

[14] J. A. Fox. Effect of water and paint coatings on laser-irradiated targets. Applied Physics Letters 24.10 (1974): 461-464.

[15] K. Liu, and E. Garmire. Paint removal using lasers. Applied optics 34.21 (1995): 4409-4415.

[16] H.C. Zhao, Y.L. Qiao, X. Du, S.J. Wang. Laser cleaning performance and mechanism in stripping of Polyacrylate resin paint. Applied Physics A 126 (2020): 1-14.

[17] J. Yang, J.H. Han, T. Duan, N.C. Sun, C. Guo, G.F. Feng. Mechanical analysis of paint film stripping from aluminum plate surface by means of nanosecond laser. Laser Technol 37 (2013): 718-722.

[18] X.K. Li, Q. Zhang, X. Zhou, D. Zhu, Q. Liu. The influence of nanosecond laser pulse energy density for paint removal. Optik 156 (2018): 841-846.

[19] Y.L. Yao, H. Chen, W. Zhang. Time scale effects in laser material removal: a review. The International Journal of Advanced Manufacturing Technology 26.5-6 (2005): 598-608.

[20] H.C. Zhao, Y.L. Qiao, Q. Zhang, X. Du, Y. Zang, X.T. Liu, B.Y. Han. Study on the characteristics and mechanism of pulsed laser cleaning of polyacrylate resin coating on aluminum alloy substrates. Applied Optics 59.23 (2020): 7053-7065.

[21] M.A. Jafarabadi, M.H. Mahdieh. Investigation of phase explosion in aluminum induced by nanosecond double pulse technique. Applied Surface Science 346 (2015): 263-269.

[22] D.N. Patel, P. K. Pandey, R. K. Thareja. Stoichiometry of laser ablated brass nanoparticles in water and air. Applied optics 52.31 (2013): 7592-7601.

[23] F. Vidal, T.W. Johnston, S. Laville, O. Barthélemy, M. Chaker, B. Le Drogoff, J. Margot, M. Sabsabi. Critical-point phase separation in laser ablation of conductors. Physical review letters 86.12 (2001): 2573.

[24] Q. H. Tang, D. Zhou, Y. L. Wang, G. F. Liu. Laser cleaning of sulfide scale on compressor impeller blade. Applied Surface Science 355 (2015): 334-340.

[25] Han, D., Xu, J., Wang, Z., Yang, N., Li, X., Qian, Y., Li, G., Dai, R., Xu, S., Penetrating effect of high-intensity infrared laser pulses through body tissue. RSC advances 8.56 (2018): 32344-32357.

[26] M. She, D. Kim, C. P. Grigoropoulos. Liquid-assisted pulsed laser cleaning using near-infrared and ultraviolet radiation. Journal of applied Physics 86.11 (1999): 6519-6524.

[27] T.G. Kim, Y.S. Yoo, S.H. Lee, J.G. Park, Effects of size, humidity, and aging on particle removal from Si wafers, Microelectron. Eng. 86 (2009) 145–149.

[28] J.H. Han, Cui X, Wang S, Feng G, Deng G, Hu R. Laser effects based optimal laser parameter identifications for paint removal from metal substrate at 1064 nm: a multi-pulse model. Journal of Modern Optics 64.19 (2017): 1947-1959.

[29] Temnov V.V., Sokolowski-Tinten, K., Zhou, P., El-Khamhawy, A., Von Der Linde, D., Multiphoton ionization in dielectrics: comparison of circular and linear polarization. Physical review letters 97.23 (2006): 237403.

[30] S. Amoruso, Modeling of UV pulsed-laser ablation of metallic targets. Applied Physics A 69.3 (1999): 323-332.

[31] Y. Lu, L.J. Yang, Y. Wang, H. Chen, B. Guo, Z. Tian. Paint Removal on the 5A06 Aluminum Alloy Using a Continuous Wave Fiber Laser. Coatings, 9(8) (2019):488.

[32] Watkins, K.; McMahon, M.; Steen, W. Microstructure and corrosion properties of laser surface processed aluminium alloys: A review. Mater. Sci. Eng. A (1997): 231, 55–61.

[33] Li, R.; Ferreira, M.; Almeida, A.; Vilar, R.; Watkins, K.; McMahon, M.; Steen, W. Localized corrosion of laser surface melted 2024-T351 aluminium alloy. Surf. Coat. Technol. (1996), 81, 290–296.

[34] W.F. Zou, Y.M. Xie, X. Xiao, X.Z. Zeng, Y. Luo. Application of thermal stress model to paint removal by Q-switched Nd: YAG laser. Chinese Physics B 23.7 (2014): 074205.

[35] V. Oliveira, and R. Vilar. Finite element simulation of pulsed laser ablation of titanium carbide. Applied surface science 253.19 (2007): 7810-7814.

[36] N.A. Vasantgadkar, U. V. Bhandarkar, S.S. Joshi. A finite element model to predict the ablation depth in pulsed laser ablation. Thin Solid Films 519.4 (2010): 1421-1430.

[37] L.Y. Yue, Z.B. Wang, L. Li. Modeling and simulation of laser cleaning of tapered micro-slots with different temporal pulses. Optics & Laser Technology 45 (2013): 533-539.

[38] C.A. Aguilar, Y. Lu, S. Mao, S. Chen. Direct micro-patterning of biodegradable polymers using ultraviolet and femtosecond lasers. Biomaterials 26.36 (2005): 7642-7649.

[39] N. Arnold, N. Bityurin, D. Bäuerle. Laser-induced thermal degradation and ablation of polymers: bulk model. Applied Surface Science 138 (1999): 212-217.

[40] Srinivasan, V., Mark A. Smrtic, S. V. Babu. Excimer laser etching of polymers. Journal of applied physics 59.11 (1986): 3861-3867.

[41] A. A. Serafetinides, C.D. Skordoulis, M.L. Maropoulou. Picosecond and subpicosecond visible laser ablation of optically transparent polymers. Applied surface science 135.1-4 (1998): 276-284.

[42] Z. B. Wang, M.H. Hong, Y.F. Lu, D.J. Wu, B. Lan. Femtosecond laser ablation of polytetrafluoroethylene (Teflon) in ambient air. Journal of applied physics 93.10 (2003): 6375-

6380.

[43] Y. Lu, L.J. Yang, M.L. Wang, Y. Wang. Simulation of nanosecond laser cleaning the paint based on the thermal stress. Optik (2020): 165589.

[44] R.R. Fang, D. Zhang, Z. Li, F. Yang, L. Li, X. Tan. Improved thermal model and its application in UV high-power pulsed laser ablation of metal target. Solid State Communications 145.11-12 (2008): 556-560.

[45] D. VonderLinde, K. Sokolowski-Tinten. The physical mechanisms of short-pulse laser ablation. Applied Surface Science 154 (2000): 1-10.

[46] Y. Lu, Y.C. Guan, Y. Li, Y. Wang, M.L. Wang. Nanosecond laser fabrication of superhydrophobic surface on 316L stainless steel and corrosion protection application. Colloids and Surfaces A: Physicochemical and Engineering Aspects 604 (2020): 125259.

[47] X.J. Wang, S.Y. Long. Study on hereditary of pores in laser remelting of die casting AZ91D magnesium alloy. Acta Metall Sin 48.12 (2012): 1437-1445.

[48] Z.M. Wang, X.Y. Zeng, W.L. Huang. Parameters and surface performance of laser removal of rust layer on A3 steel. Surface and Coatings Technology 166.1 (2003): 10-16.

[49] Y. Cui, J.Q. Shen, S.S. Hu. Microstructure and performance of the laser melted aluminum bronze layers with and without using activator. Materials Research Express 6.6 (2019): 066513.

[50] Y. He, J. Wei, J.Y. Liu, Y. Wang. Experimental study on the fabrication profile and mechanical properties by substrate-inclined angle using laser melting deposition (LMD) integrating with the

substrate of stainless steel. Optics & Laser Technology 125 (2020): 106038.

[51] W.D. Nix. Mechanical properties of thin films. Metallurgical transactions A 20.11 (1989): 2217.

[52] J.J. Lewandowski, M. Seifi. Metal additive manufacturing: a review of mechanical properties. Annual review of materials research 46 (2016).

[53] B.X. Su, B. Wang, L. Wang, Y. Su, F. Wang. The corrosion behavior of Ti-6Al-3Nb-2Zr-1Mo alloy: effects of HCl concentration and temperature. Journal of Materials Science & Technology (2020).

[54] B.X. Su, L. Luo, B. Wang, Y. Su, L. Wang. Annealed microstructure dependent corrosion behavior of Ti-6Al-3Nb-2Zr-1Mo alloy. Journal of Materials Science & Technology 62 (1920): 234-248.

[55] V. Crupi, E. Gulielmino, M. Maestro, A. Marino. Fatigue analysis of butt welded AH36 steel joints: thermographic method and design S–N curve. Marine Structures 22.3 (2009): 373-386.

[56] J. Cheon, D.V. Kiran, S.J. Na. Thermal metallurgical analysis of GMA welded AH36 steel using CFD–FEM framework. Materials & Design 91 (2016): 230-241.

[57] G.X. Zhang, X.M. Hua, Ye Huang, Y.L. Zhang, Fang Li, Chen Shen, Jian Cheng. Investigation on mechanism of oxide removal and plasma behavior during laser cleaning on aluminum alloy. Applied Surface Science 506 (2020): 144666.

[58] David Gaskel, Introduction to the Thermodynamics of Materials, fourth ed., Taylor & Francis,

2003.

FIGURE LIST

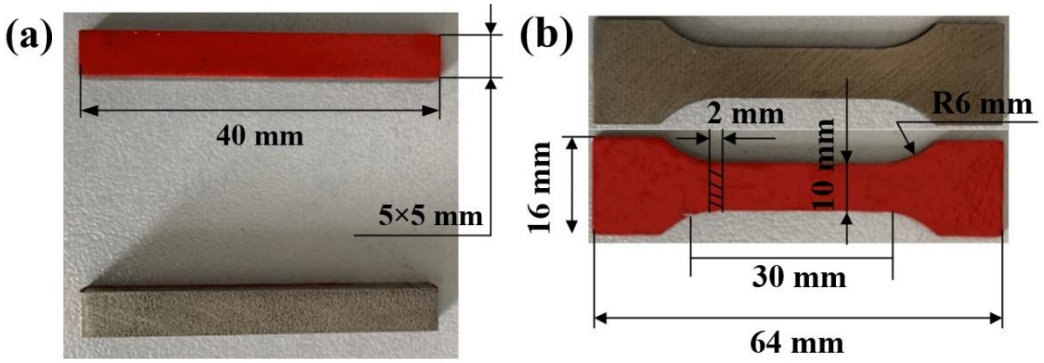

Fig. 1. (a) Standard Tensile Samples (b) standard Bending Samples.

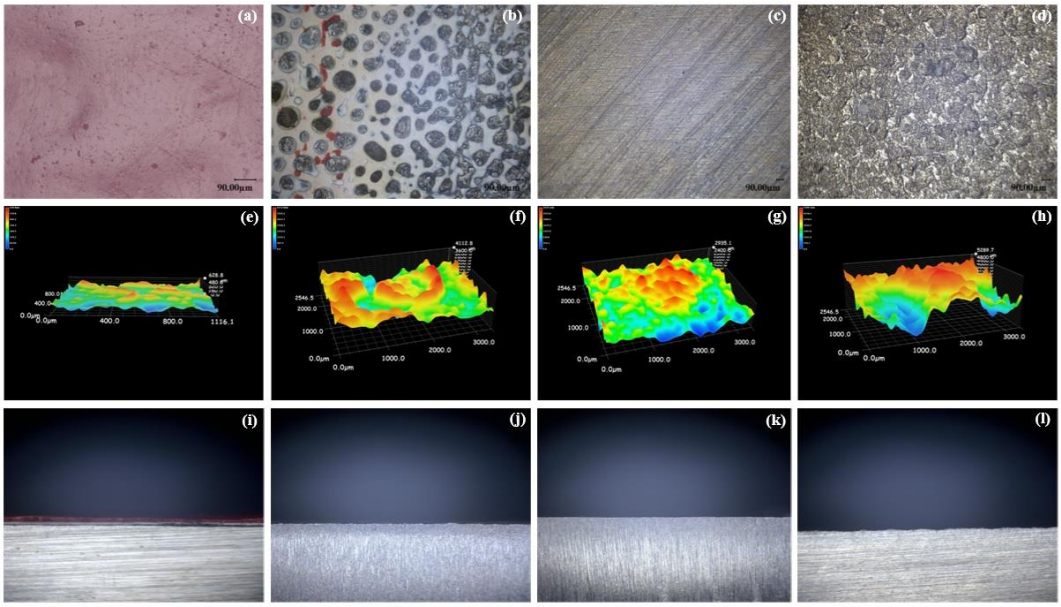

Fig. 2. Macroscopic three- and two-dimensional optical images of original surface (a, e, i) and laser cleaned surface at scanning speed of 1000 mm/s with different fluence, among them (b, f, j) at laser fluence of 2 J/cm^2, (c, g, k) at laser fluence of 5 J/cm^2, (d, h, l) at laser fluence of 7 J/cm^2 respectively.

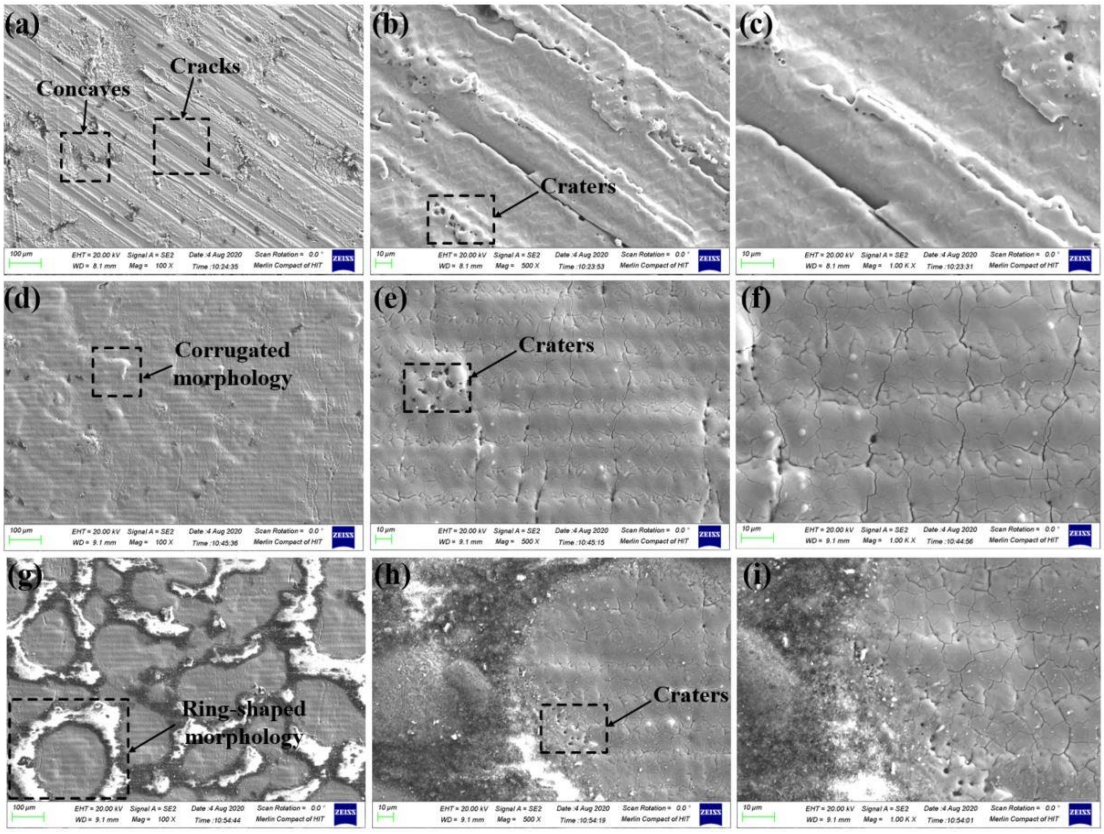

Fig. 3. SEM images of laser cleaned surface at different fluence (a) 2 J/cm^2 (d) 5 J/cm^2 (g) 7 J/cm^2, (b, c), (e, f) and (h, i) are the accordingly magnification images, correspondingly.

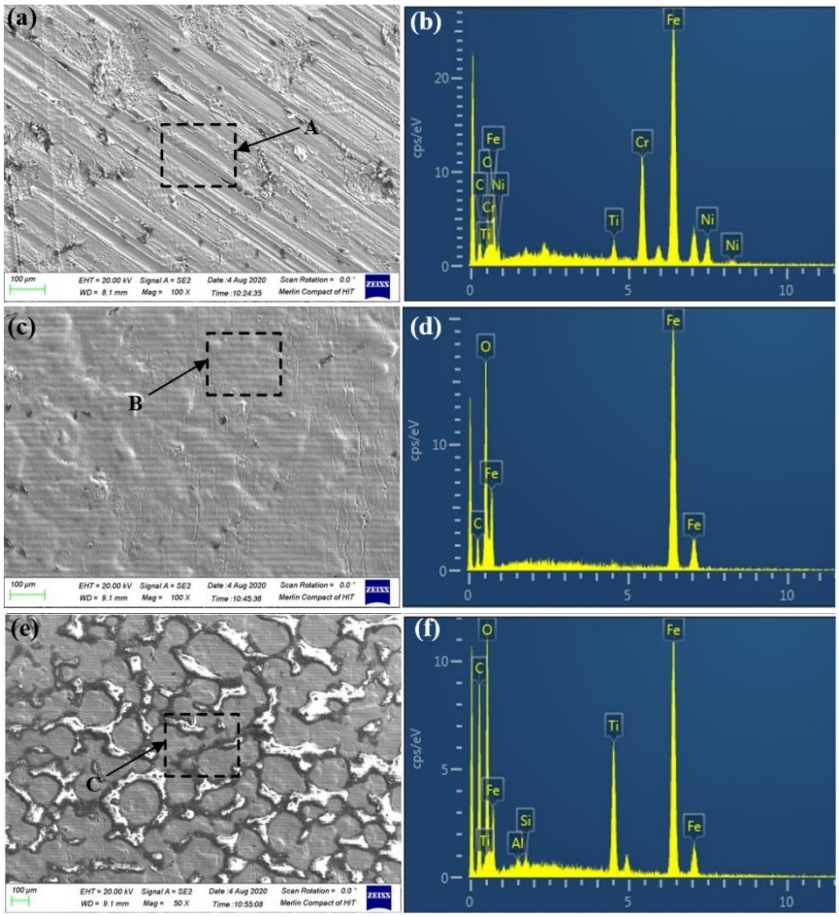

Fig. 4. SEM and EDS images of laser cleaned surface with various fluence (a) 2 J/cm^2 (c) 5 J/cm^2 (e) 7 J/cm^2, (b)–(f) are the accordingly EDS images, respectively.

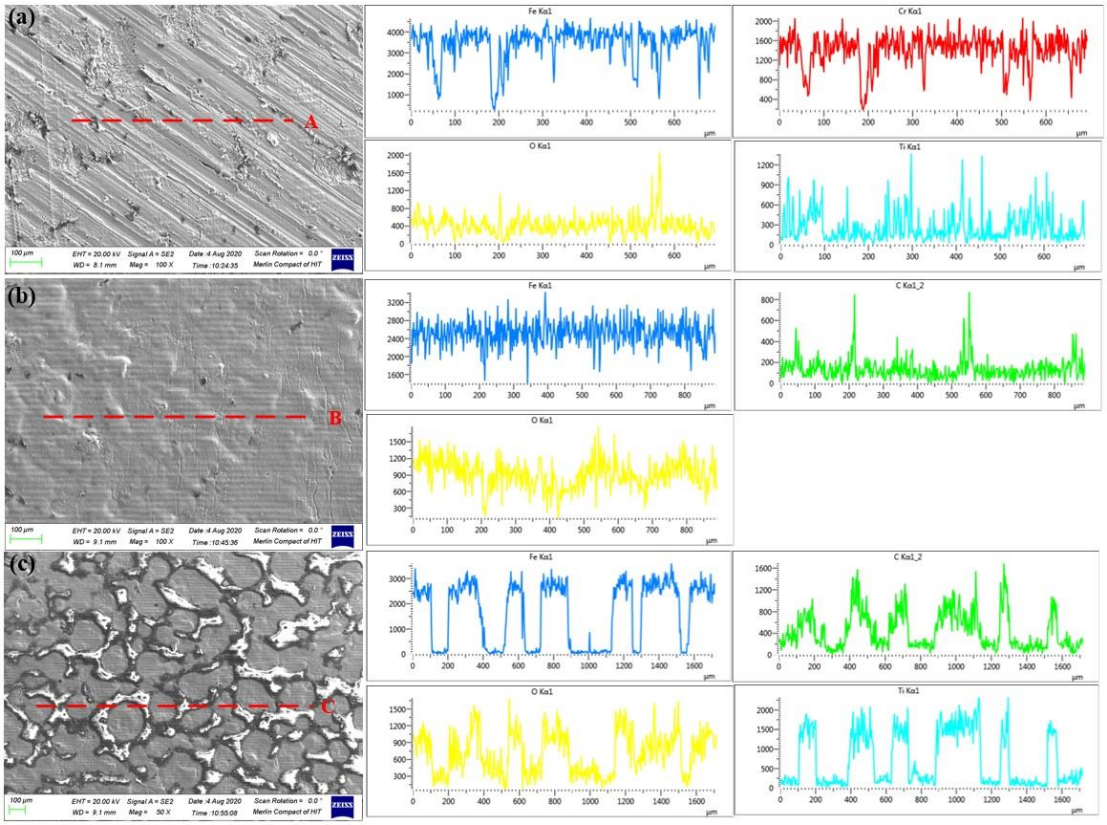

Fig. 5. Line EDS images of laser cleaned surface with different laser fluence (a) 2 J/cm^2 (b) 5 J/cm^2 (c) 7 J/cm^2, respectively.

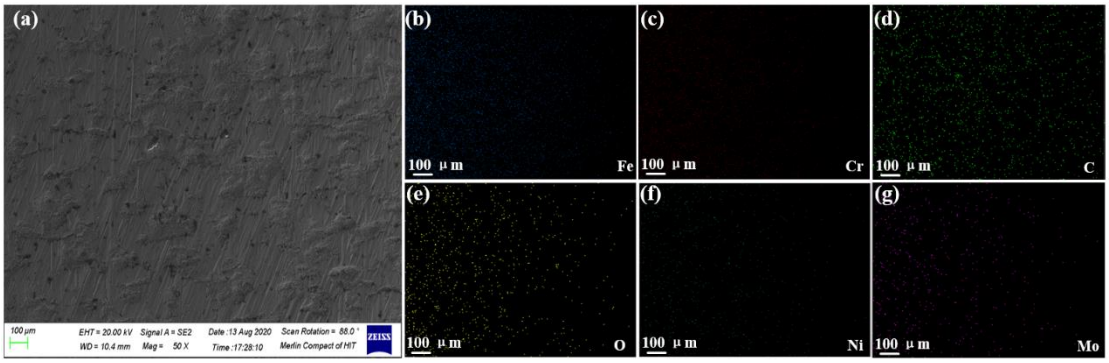

Fig. 6. SEM images of laser cleaned surface and (b)–(g) are the accordingly elemental distributions after laser cleaning, respectively.

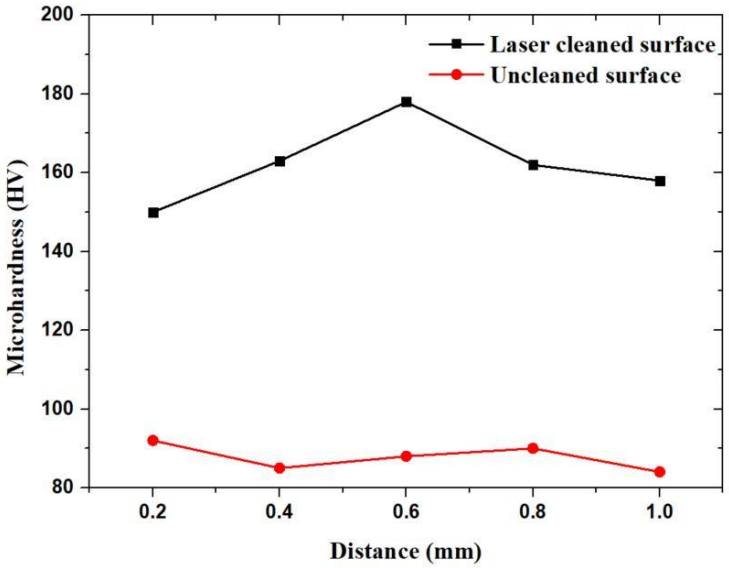

Fig. 7. The microhardness characterization after UV laser cleaning.

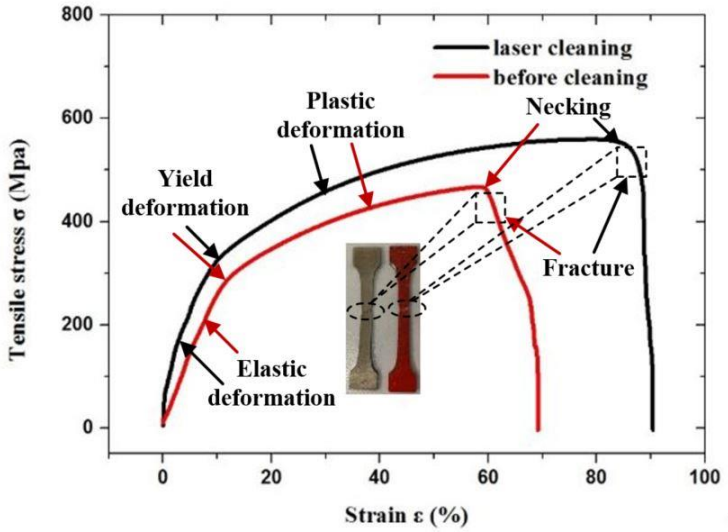

Fig. 8. The relationship between the strain and tensile stress.

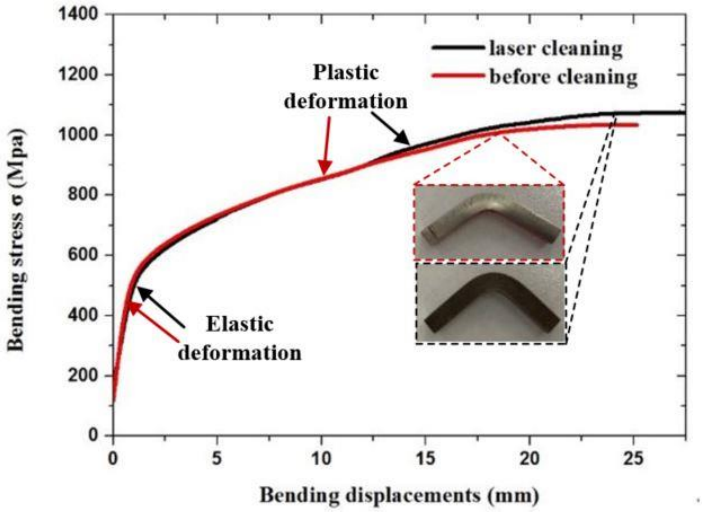

Fig. 9. The relationship between the bending displacements and bending stress.

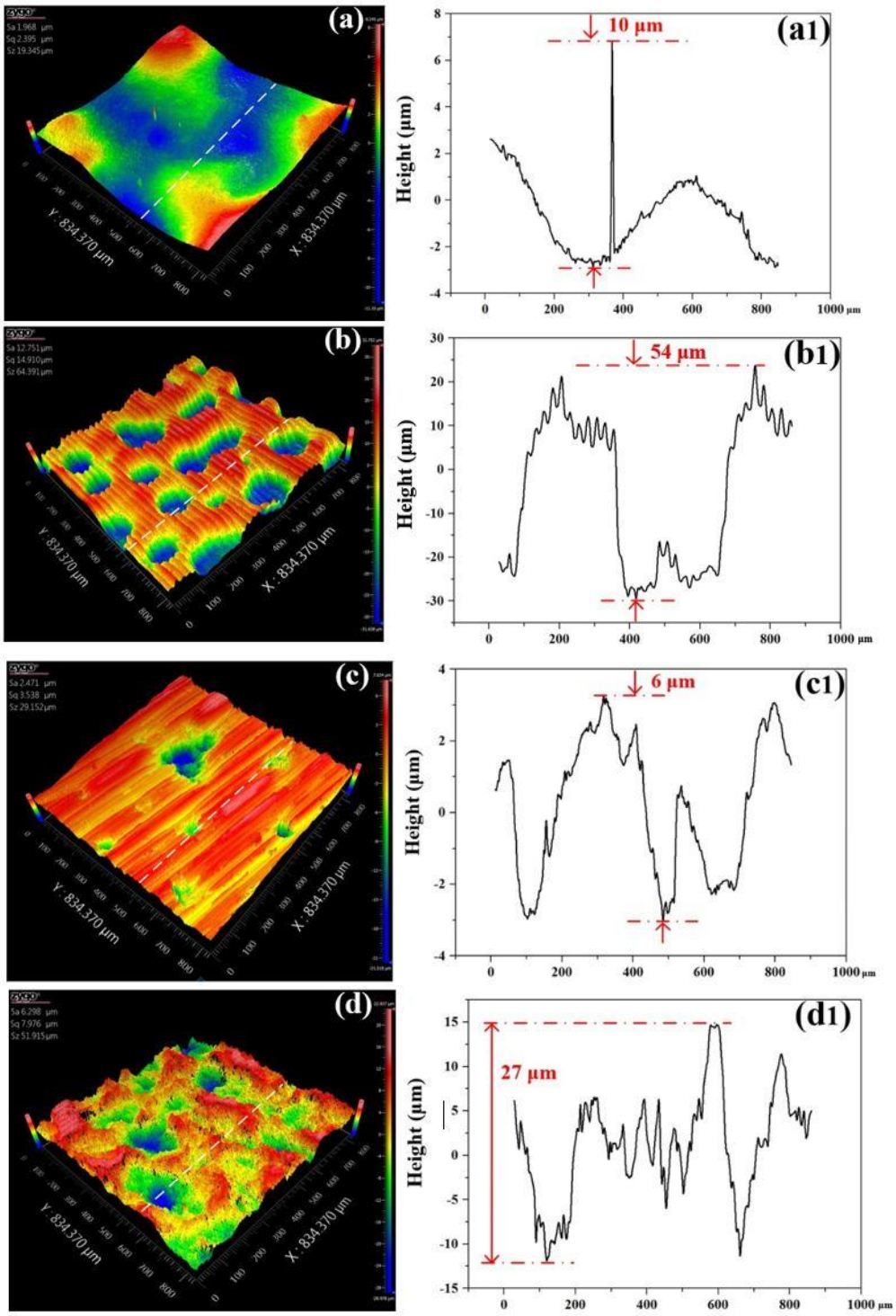

Fig. 10. Optical profiler 3D height images of laser cleaned painting layer surfaces (a) original painting layer (b) laser cleaned surface at laser fluence 2 J/cm^2 (c) 5 J/cm^2 (d) 7 J/cm^2, (a1)–(d1) are the accordingly line scanned profiles, respectively.

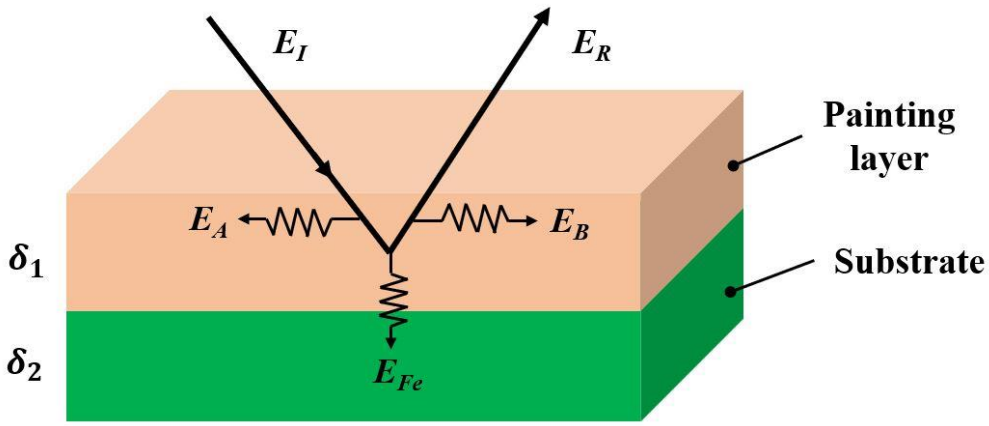

Fig. 11. Schematic diagram of laser cleaning painting layer model.

TABLE LIST

Table 1. Mass fraction of elements in AH36 steel w%.

Elements	Fe	Mn	Si	C	P	S
Mass fraction	base	1.20-1.45	0.15-0.50	0.15-0.18	0.025	0.1

Table 2. Chemical bond energies of painting layer.

Polymer bonds	C-N	C-H	C=C	O-O	C=O	C-C
Bond energy	3.04	4.30	8.44	5.12	6.40	3.62

Table 3. The element composition measured by EDS of the laser cleaned painting layer surface with 3 different areas.

element	A	B	C
	Weight/%	Weight/%	Weight/%
C	17.41	12.89	30.67
O	5.58	24.50	27.67
Fe	53.04	62.61	32.43

Table 4. The physical constants of Fe substrate and painting layer [58].

	substance	M	ρ(g/cm^3)	Melting point(℃)	Boiling point(℃)
Physical constants	Fe substrate	56	7.87	1535	3000
	Painting layer	92.5	1.30	648	789.5

	substance	Transition	ΔH, J	T, K
Phase transition constants	Fe substrate	s→l	13770	1809
	Fe substrate	l→g	27480	2563
	Painting layer	s→l	9650	3003

	substance	a	b	c	Range, K
Heat capacity constants	Fe substrate$_{(s)}$	37.12	617	0	298-1809
	Fe substrate$_{(l)}$	41.8	0	0	1809-1873
	Painting layer	121.46	8.54	-19.16	298-937

Figures

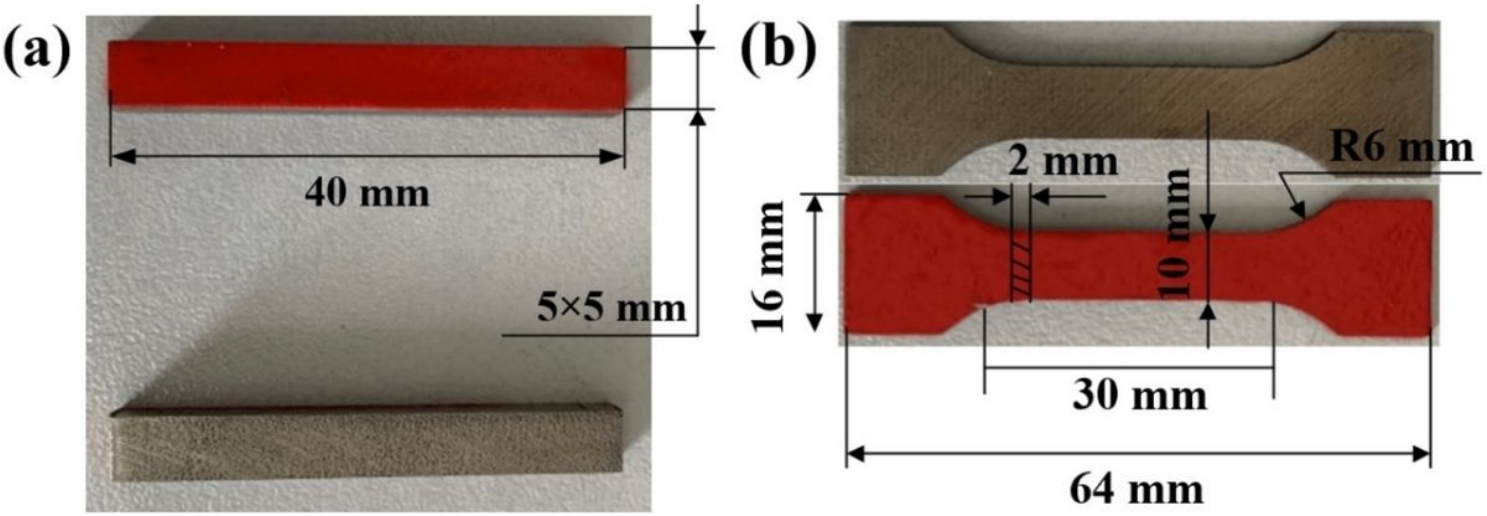

Figure 1

(a) Standard Tensile Samples (b) standard Bending Samples.

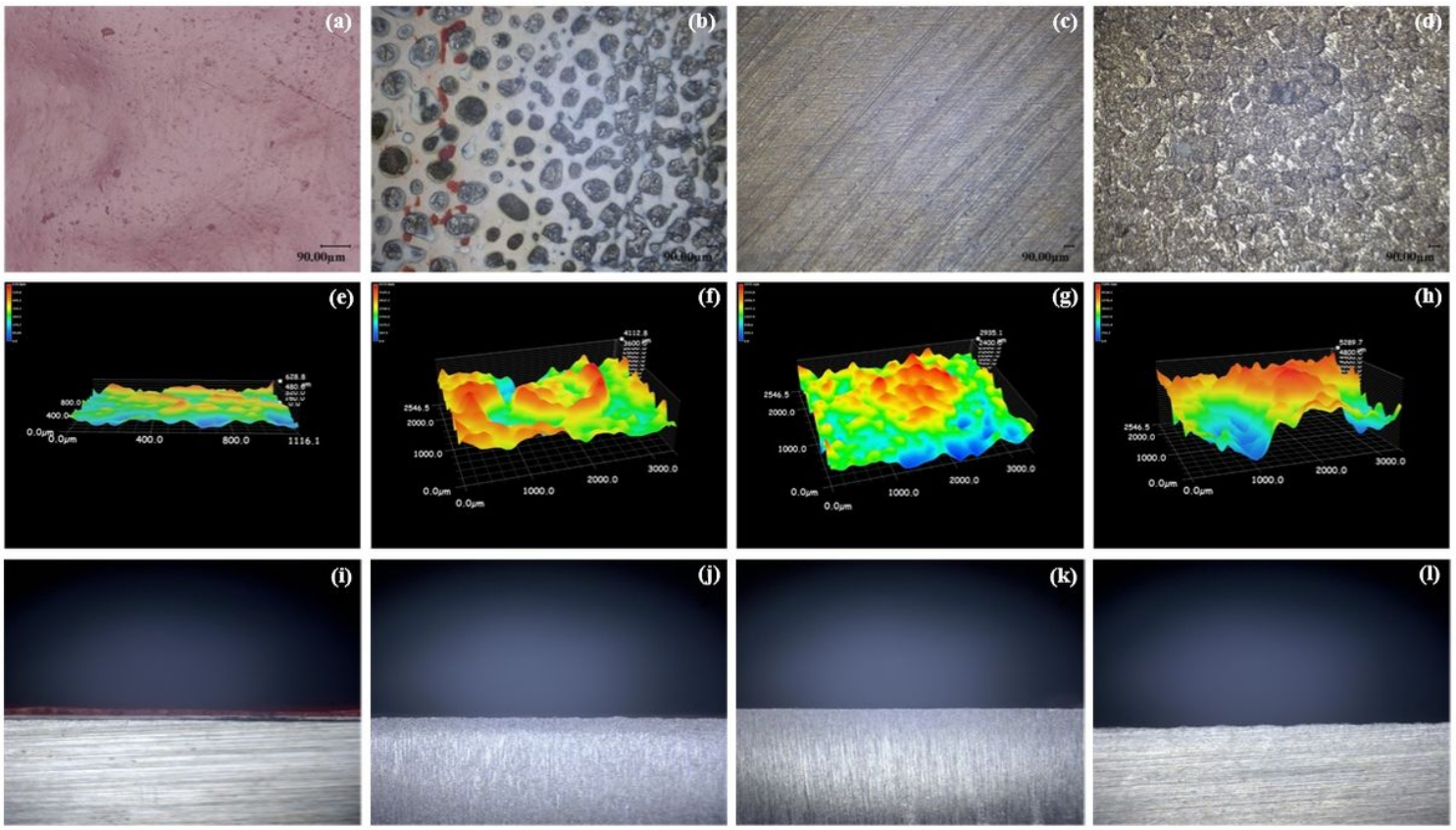

Figure 2

Macroscopic three- and two-dimensional optical images of original surface (a, e, i) and laser cleaned surface at scanning speed of 1000 mm/s with different fluence, among them (b, f, j) at laser fluence of 2 J/cm2, (c, g, k) at laser fluence of 5 J/cm2, (d, h, l) at laser fluence of 7 J/cm2 respectively.

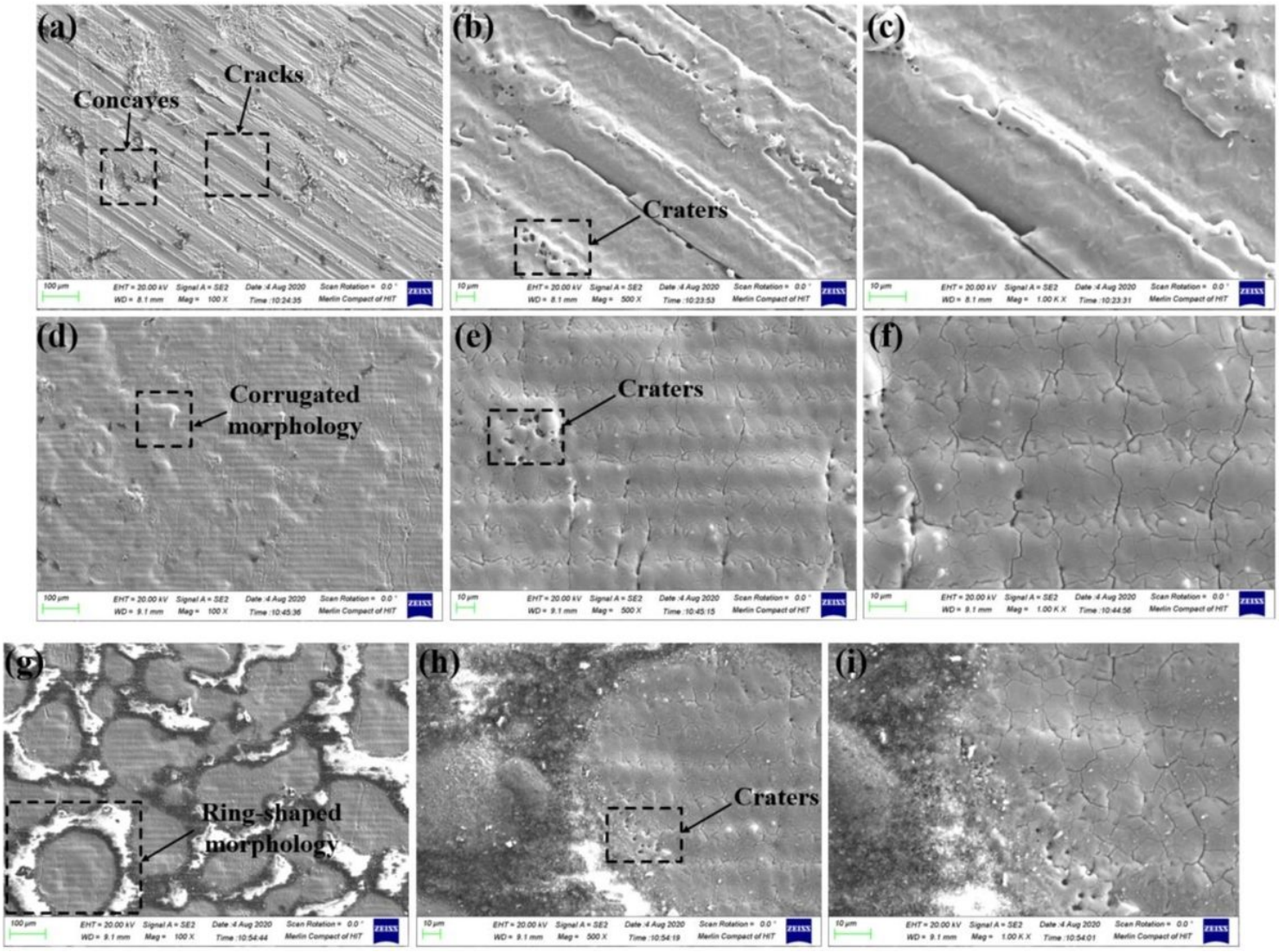

Figure 3

SEM images of laser cleaned surface at different fluence (a) 2 J/cm2 (d) 5 J/cm2 (g) 7 J/cm2, (b, c), (e, f) and (h, i) are the accordingly magnification images, correspondingly.

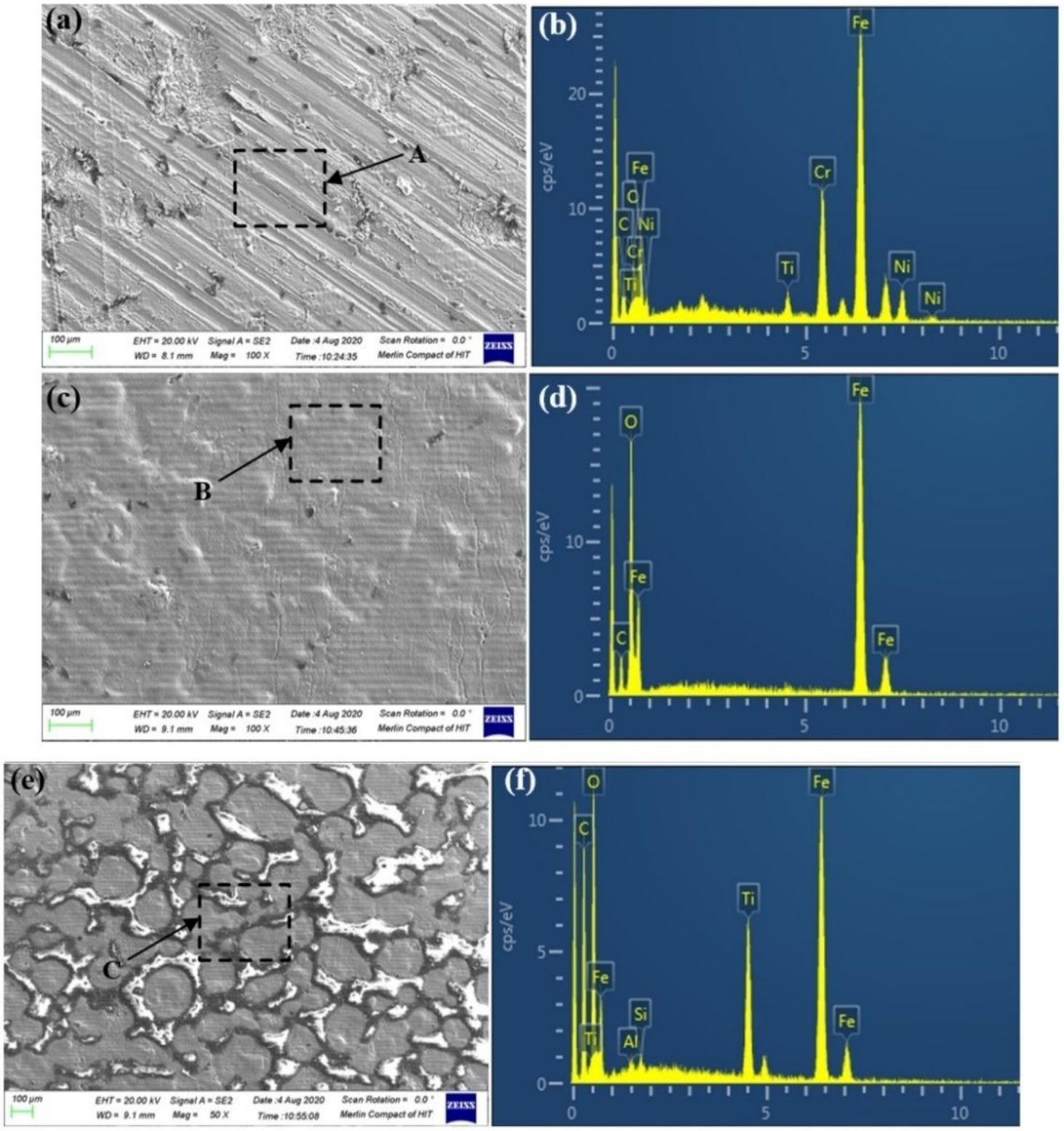

Figure 4

SEM and EDS images of laser cleaned surface with various fluence (a) 2 J/cm2 (c) 5 J/cm2 (e) 7 J/cm2, (b)–(f) are the accordingly EDS images, respectively.

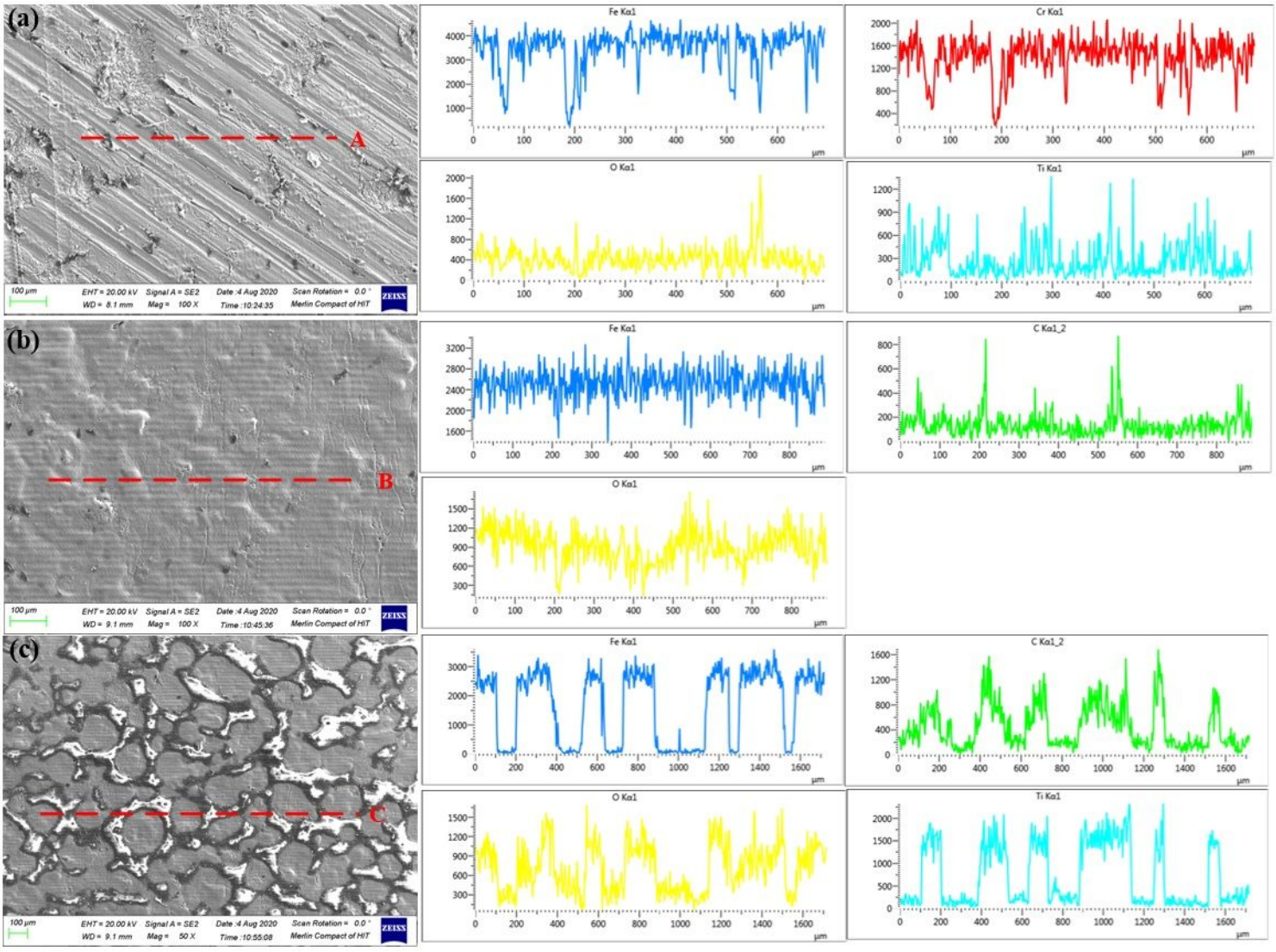

Figure 5

Line EDS images of laser cleaned surface with different laser fluence (a) 2 J/cm2 (b) 5 J/cm2 (c) 7 J/cm2, respectively.

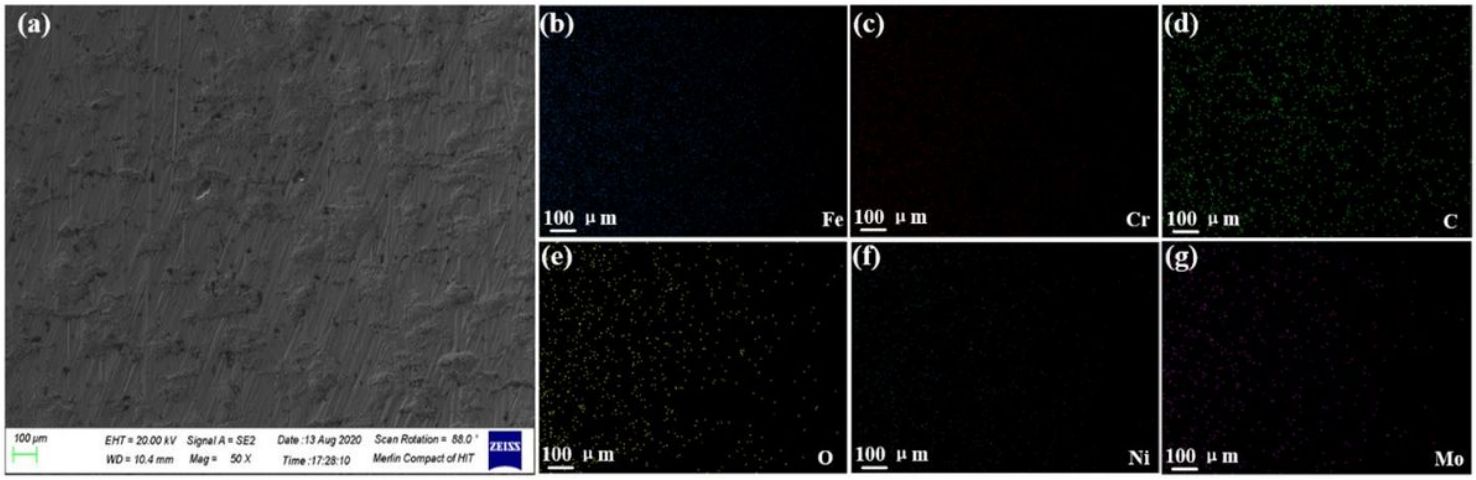

Figure 6

SEM images of laser cleaned surface and (b)–(g) are the accordingly elemental distributions after laser cleaning, respectively.

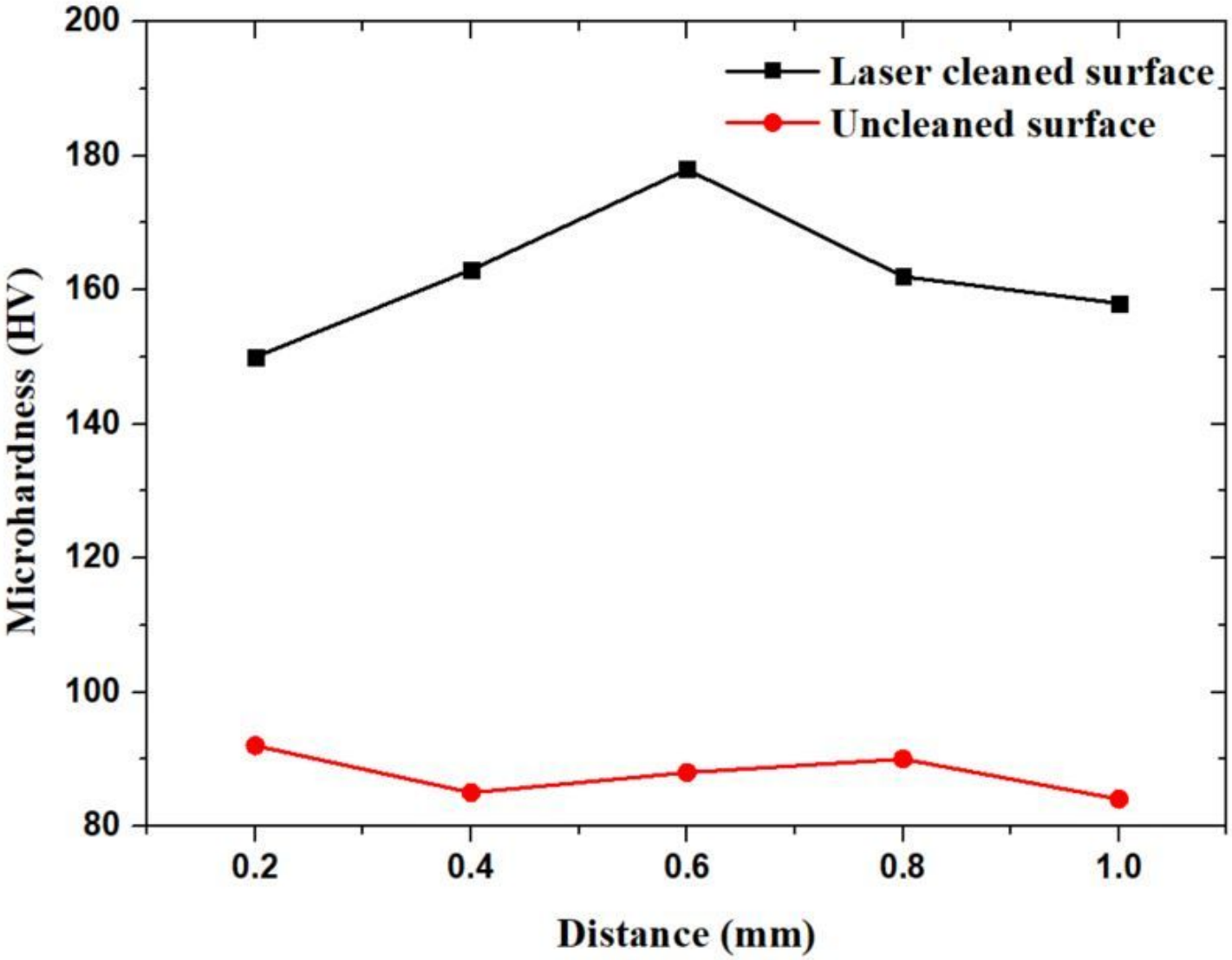

Figure 7

The microhardness characterization after UV laser cleaning.

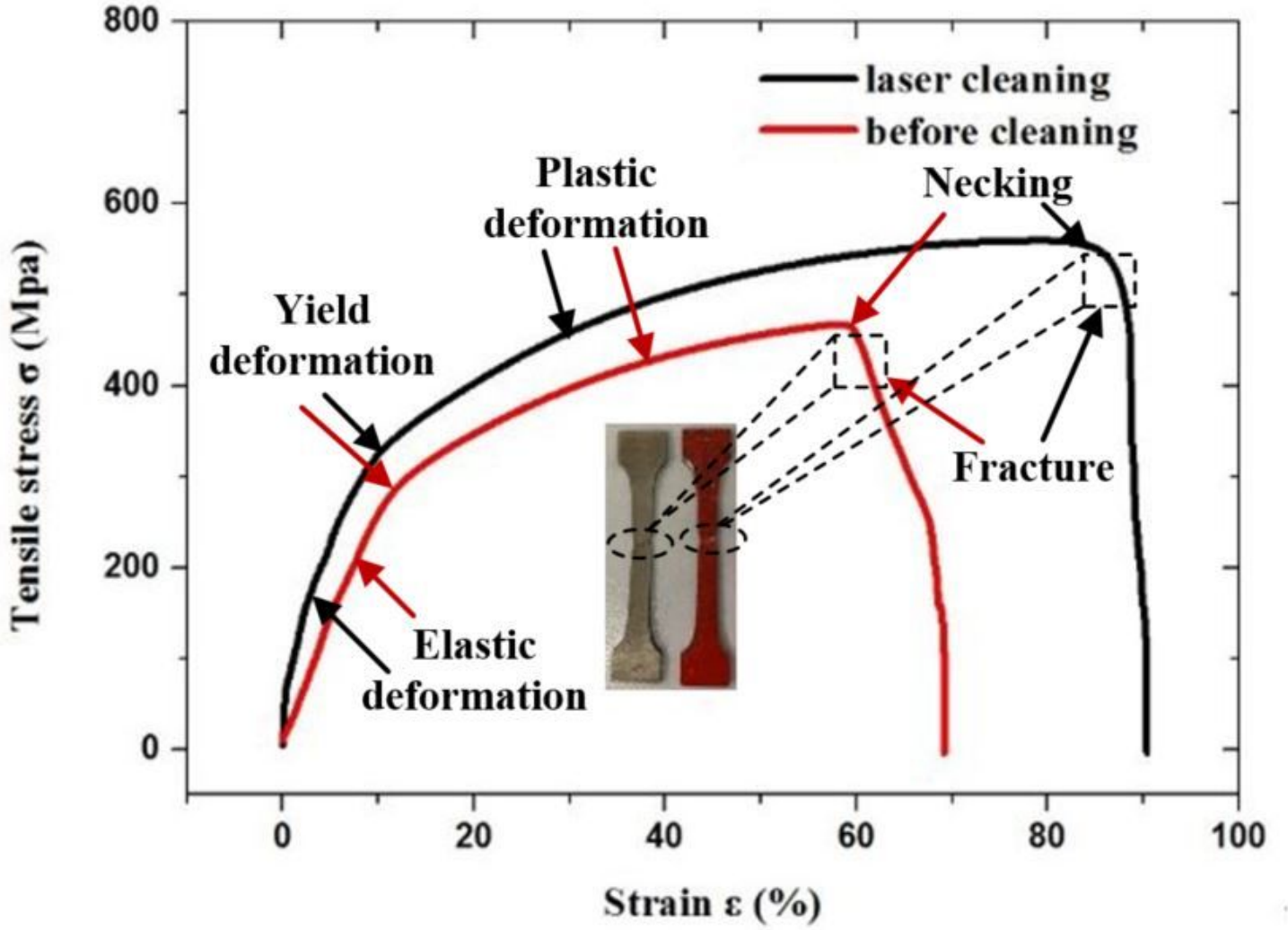

Figure 8

The relationship between the strain and tensile stress.

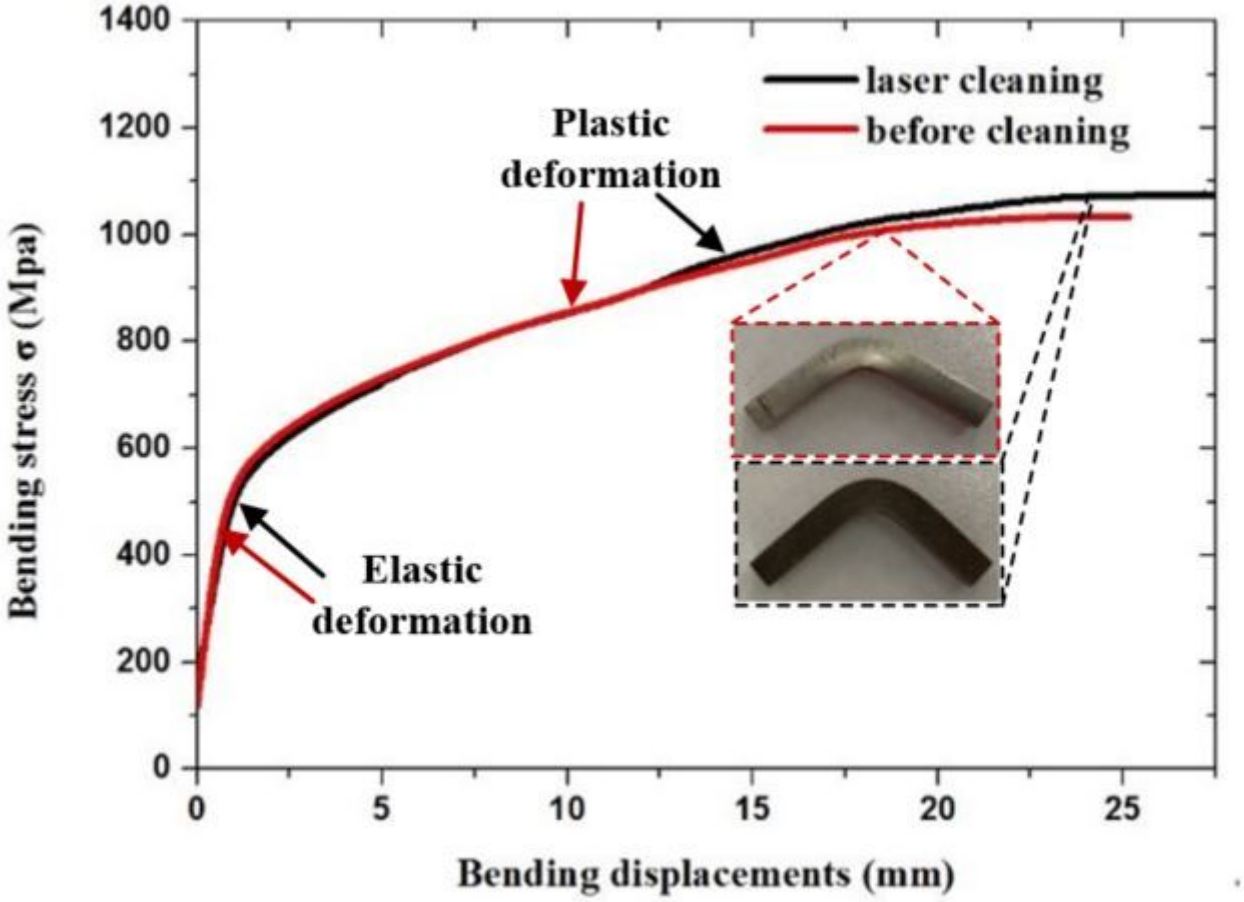

Figure 9

The relationship between the bending displacements and bending stress.

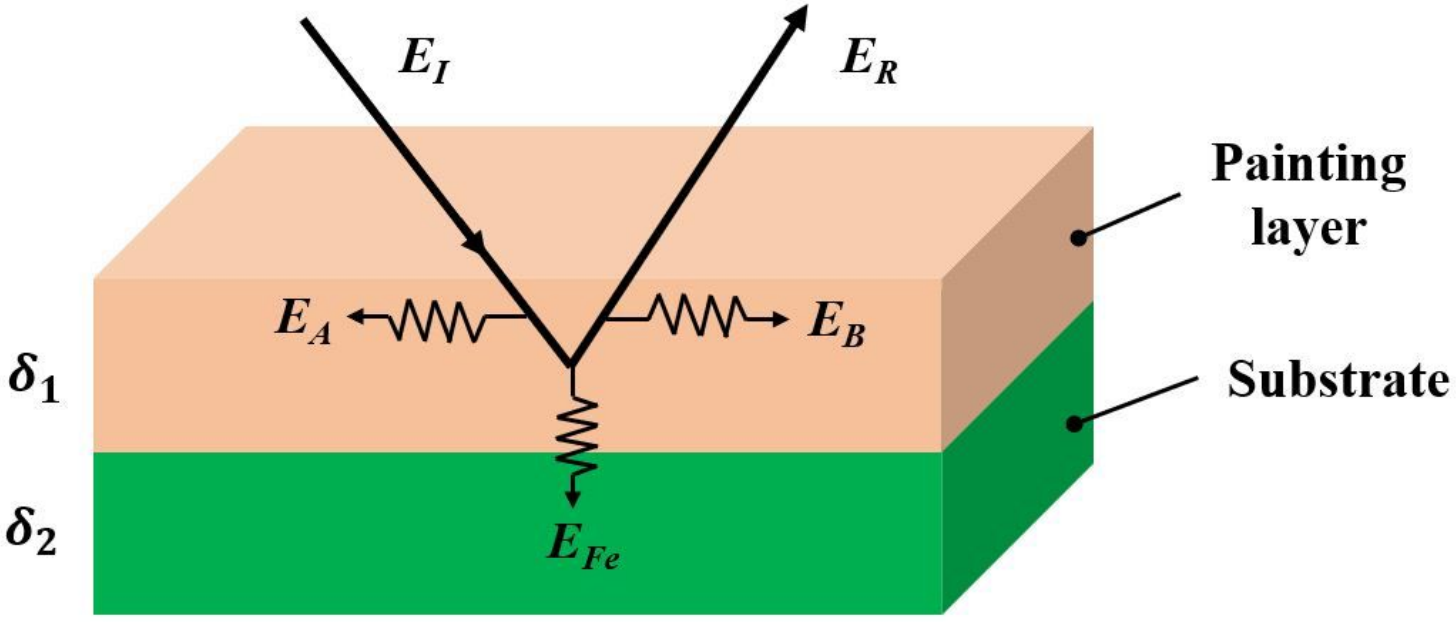

Figure 11

Schematic diagram of laser cleaning painting layer model.